Electronic structure and X-ray absorption spectrum of rutile TiO_2

1991 J. Phys.: Condens. Matter 3 8195

(http://iopscience.iop.org/0953-8984/3/42/014)

J. Phys.: Condens. Matter 3 (1991) 8195–8204. Printed in the UK

Electronic structure and x-ray absorption spectrum of rutile TiO_2

B Poumellec†, P J Durham‡ and G Y Guo‡

† CNRS-UA446, CNS UPS, Batiment 415 91405 Orsay Cédex, France

‡ SERC Daresbury Laboratory, Warrington WA4 4AD, UK

Received 29 August 1990, in final form 16 July 1991

Abstract. The electronic band structure of rutile TiO_2 has been calculated using the linear muffin-tin orbital (LMTO) method. The x-ray absorption spectrum has also been obtained from the calculated band structure and self-consistent potential. The dipole as well as the quadrupole contribution to the x-ray absorption spectrum has been calculated. The calculated band structure shows that there is a significant 2p (O)–3d (Ti) mixing in the valence band which, however, becomes weaker in the Ti d-dominated conduction band. The valence band is well separated from the conduction band by a direct energy gap which is almost degenerate with the indirect energy gap. A comparison with experiments suggests that the majority of the observed pre-edge and edge features in the Ti K-edge x-ray absorption spectrum are due to 1s → 4p dipole transitions, a result of the small Ti–Ti (3d–4p) hybridization in the conduction band region. The quadrupole transition contribution is found to be insignificant.

1. Introduction

TiO_2 is an oxide of considerable technological interest. Stoichiometric TiO_2 is an insulator. However, it becomes a conductor when it is slightly reduced. TiO_2 has been widely used in catalysis, electrochromism and sensors [1]. Its chemical properties have been extensively studied but its electronic properties have not. Many authors refer to the electronic band structure of perovskite $SrTiO_3$ because no first principles calculation of TiO_2 band structure had been reported. However, because the structure of TiO_2 is different from that of $SrTiO_3$, the band structures of TiO_2 and $SrTiO_3$ may be quite different.

The optical (and thermal) band gap of TiO_2 is large (3 eV) [2]. It is often assumed that pure TiO_2 is an ionic insulator. Thus, one would expect that TiO_2 has a valence band of purely O 2p character and a conduction band predominated by the Ti 3d orbitals. It is of interest to investigate the electronic structure of TiO_2 and hence the validity of this assumption.

Two band structure calculations have been published [3, 4], both based on the empirical tight binding method. In this work, we have performed self-consistent band structure calculations for TiO_2 from first principles. The calculated site and angular momentum (L) decomposed density of states (DOS) were then used to calculate x-ray absorption spectrum (XAS) within the electric dipole approximation. To help to understand the origins of some pre-edge features in the observed Ti K-edge x-ray absorption spectrum, we have also calculated the contribution due to the electric

0953-8984/91/428195+10$03.50

quadrupole transitions using the self-consistent potentials generated by the band structure calculations. In this article, we present the band structure, density of states, and theoretical x-ray absorption spectrum. We also compare our results with, mainly, x-ray absorption experiments and try to identify the origin and nature of the puzzling pre-edge features in the experimental Ti K-edge x-ray absorption spectrum.

The arrangement of this article is as follows. In section 2 the details of the band structure calculation are given. The results of the band structure calculations are then presented in section 3. In section 4, after describing briefly how we evaluate the x-ray absorption spectrum from the obtained Ti p-projected density of states (p-DOS), we report and compare the calculated x-ray spectrum with experiments. Some concluding remarks are presented in section 5.

2. Details of band structure calculation

The rutile structure of TiO_2 (shown in figure 1(a)) is a simple tetragonal lattice with a basis of two formula units per cell. The symmetry properties of this rutile structure (described by space group D_{14}^{4h}) have been discussed in [5] and that notation is used here. The coordinates of the basis are given in table 1 [6]. Each Ti atom is surrounded by six O atoms in a distorted octahedral coordination (TiO_6), in contrast to the regular octahedron TiO_6 in $SrTiO_3$. The bond length (d_2) between Ti and two of the six Os in the octahedron is $\sqrt{2}ua$ and the bond length (d_2) between Ti and the other four Os is given by

$$d_2 = \left[2\left(\frac{1}{2}-u\right)^2 + \left(\frac{c}{2a}\right)^2\right]^{1/2} a$$

where $c/a \neq 2u$ since the TiO_6 octahedron is distorted.

The self-consistent band structure of TiO_2 has been calculated using the LMTO method with the atomic sphere approximation (ASA) [7]. The calculations are based on the density functional theory with the local density approximation. The standard local exchange-correlation potential of von Barth–Hedin [8] is used. The LMTO-ASA method assumes spherically symmetric potentials inside overlapping atomic spheres. It is very fast and accurate for closely packed solids (see [7] for details). Because of its speed, the LMTO-ASA method is particularly useful for large and complex systems, such as TiO_2. The rutile structure of TiO_2 is rather open. To reduce the overlap of the atomic spheres and minimize the error due to the ASA, we introduce four so-called empty spheres (or 'vacancy' spheres) into the interstitial region at the positions listed in table 1. The atomic radii chosen are 1.327, 1.111 and 1.058 Å, respectively for Ti, O and 'empty' spheres (the overlapping volume is only about 17%). The basis functions are s, p, d LMTOs for Ti and O, and s, p LMTOs only for 'empty' spheres. In the Ti sphere, the 4f state lies about 30 eV above the Fermi level. Thus, the Ti 4f state is not important here and is neglected. All the energy parameters including Ti 4p are set to the corresponding gravity centres of the occupied bands. This choice of the energy parameters should give good self-consistent potentials, valence bands and lower conduction bands (conduction bands within about 15 eV above the Fermi energy). The density of states is calculated from the obtained energy bands by the tetrahedron technique [9]. A mesh of 135 k-points within the irreducible wedge (1/16) of the tetragonal Brillouin zone (see figure 1(b)) is used. We have varied the atomic

Table 1. Crystallographic data (taken from [6]): $a = b = 4.594$ Å; $c = 2.958$ Å; $u = 0.3053$.

Atomic positions	x	y	z
Ti_1	0	0	0
Ti_2	0.5	0.5	0.5
O_1	u	u	0
O_2	$1-u$	$1-u$	0
O_3	$0.5-u$	$0.5-u$	0.5
O_4	$0.5+u$	$0.5-u$	0.5
I	0	0.5	0
I	0.5	0	0
I	0.5	0	0.5
I	0	0.5	0.5

$2 \times (TiO) = 1.984$ Å

$4 \times (TiO) = 1.946$ Å

Two distortion parameters p and e are defined as

$$p = \frac{O_1\text{-}O_2}{O_1\text{-}O_1^c} = \frac{(1-2u)\sqrt{2}}{c/a} = 0.855$$

$$e = \frac{Ti_2\text{-}O_3}{Ti_2\text{-}O_1} = \left[\left(\frac{1}{2u}-1\right)^2 + \frac{1}{2}\left(\frac{c}{a}\right)^2\right]^{-1} = 1.020$$

$c/a = 0.644$

NB: the ideal values are: $p = e = 1$; $c/a = 2u$; $u = 0.293$.

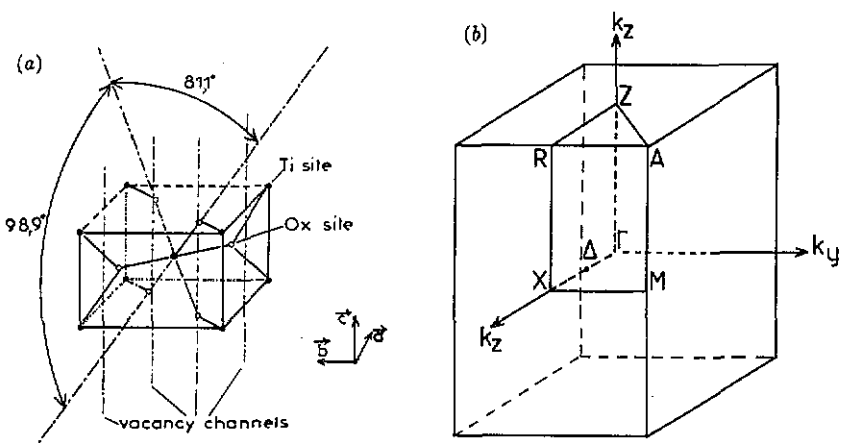

Figure 1. (*a*) Crystal structure of rutile TiO_2. (*b*) The corresponding tetragonal Brillouin zone.

radii by about 5% and found that the calculated energy bands and density of states do not change significantly.

3. Description of band structure

3.1. Valence band

The self-consistent band structure of TiO_2 is shown in figure 2 and the corresponding total density of states, site and *L*-decomposed DOS are plotted in figure 3. The valence bands are shown in the lower part of figure 2(*a*) (the O 2s bands, not shown, lie about 10 eV below the bottom of the valence bands). The 12 valence bands of largely oxygen p-like character are complicated due to the large number of the valence electrons in the unit cell. As shown in figure 3(*a*), the valence DOS consists of about two-thirds oxygen and one third titanium. Therefore, there is a strong Ti–O mixing, especially near the bottom of the valence band (figure 3(*a*)). From the *L*-decomposed Ti–DOS (figure 3(*b*)), it is found that the Ti part belongs to the d-symmetry. Nevertheless, at the top of the valence band, this mixing is weak and one may think of the electronic holes as being mainly O 2p states residing on the O sites. Finally, negligible DOS is found in the 'vacancy' spheres.

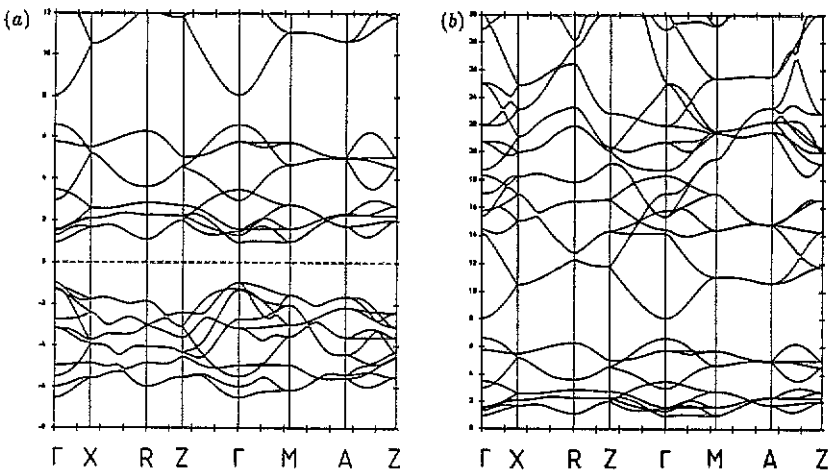

Figure 2. TiO_2 band structure: (*a*) around the Fermi level; (*b*) above the Fermi level.

3.2. Conduction band

The conduction bands are shown in the middle of figure 2(*a*). They are well separated from the valence bands and also from the higher conduction bands. The energy gap between the valence and conduction bands is about 2 eV, in reasonable agreement with experiments. The energy gap is direct and situated at the centre of the Brillouin zone (Γ point). However, there is an indirect energy gap from the Γ point of the valence band to the M point of the conduction band, of almost the same energy, and this may explain the results of many experimental studies of the type of the energy gap. We found that the indirect energy gap is about 0.03 eV wider than the direct one, in good agreement with experiments. For example, the observed energy difference between the direct and indirect gaps is 0.02 eV [10,11]. However, our results do not corroborate

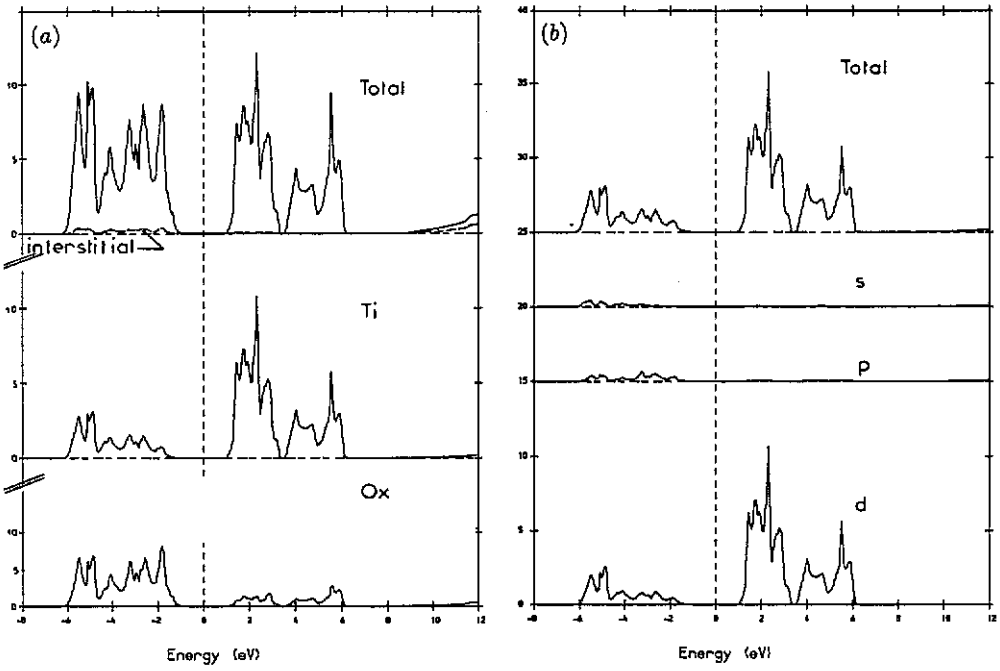

Figure 3. (*a*) Site-decomposed and (*b*) Ti *L*-decomposed DOS functions around the Fermi level.

the result that the indirect phonon-assisted gap is from A_3 to Γ_1 point [12]. The conduction bands have most of their weight on the Ti sites. Figure 3(*b*) shows that the Ti 3d orbital is almost the only component, in contrast with the valence bands described earlier. Figures 2(*a*) and 3(*a*) indicate that the conduction bands may be divided into two parts. The lower part contains six bands and the upper part contains four bands. This separation of the Ti 3d dominated conduction bands is due to the octahedral coordination of Ti by the oxygen atoms (the so-called 'crystal field' effect). Again, the DOS in the 'vacancy' spheres is small.

3.3. Higher conduction band

The higher conduction bands (figure 4(*a*)) are quite different from those reported previously [3]. Since the wavefunction is extended in this energy range, the O–Ti mixing increases rapidly as the energy is increased. The mixing is almost complete (i.e. 50% of O and 50% of Ti) about 12 eV above the Fermi level. Furthermore, there is now a significant DOS in the 'vacancy' spheres. Another interesting result is that the Ti s-partial DOS appears to be concentrated (in energy) near the bottom of this conduction band. Similarly, the p-DOS is concentrated in the energy range between 15 and 22 eV above the Fermi level (figure 4(*b*)). About 22 eV above the Fermi level, only the d-DOS is discernible. This seems to be erroneous because we know that as the energy further increases, the p-DOS should reach the p-decomposition of the plane wave in terms of spherical harmonics centred at the Ti site. As noted in the previous section, this is due to the linear (energy) approximation used in the LMTO–ASA method. Note that the energy parameters were set to the gravity centres of the

occupied bands, a few eV below the Fermi level. Nevertheless, the calculated bands and DOS functions below 15 eV should be reliable. This is sufficient for us to discuss the features in the pre-edge and edge regions in the x-ray absorption spectrum later.

4. X-ray absorption spectrum

4.1. Calculation

We have calculated x-ray absorption spectra for TiO_2 using the site and L-decomposed DOS and the self-consistent LMTA–ASA potentials (converted into non-overlapping muffin-tin form). Before presenting the theoretical x-ray absorption spectrum, we summarize the main points concerning the method we used in the present calculations (see [13] and [12] for more details).

Within the electric dipole approximation, the absorption cross section may be expressed with the oscillator strength, F_c, (in CGS units) at energy $E = E_c + h\omega$ (see appendix 2 in [14])

$$\mu(E) = 4\pi^2 h\alpha F_c(E) \tag{1}$$

where

$$F_c(E) = \frac{\omega}{3}\frac{2J+1}{2(2L+1)}\left[\frac{L}{2L-1}f_{c,L-1}(E) + \frac{L+1}{2L+1}f_{c,L+1}(E)\right]$$

and $c = (n, L, J)$, represents the core level quantum numbers (with the spin–orbit coupling neglected). For absorption at the Ti K-edge ($n = 1, L = 0, J = \frac{1}{2}$), F_c may be written simply as

$$F_c(E) = \frac{\omega}{3}f_{c,1}(E) = \frac{\omega}{3}f_{s,p}(E). \tag{2}$$

Furthermore, $f_{s,p}$ can be expressed in terms of the p-projected DOS ($N_p(E)$), i.e.

$$f_{s,p}(E) = \frac{|\langle\Phi_s|r|\Psi_p\rangle|^2}{\langle\Psi_p \,||\, \Psi_p\rangle}N_p(E) \tag{3}$$

where Ψ_s is a solution of the radial Schrödinger equation for the target atom s-core state. Inside the muffin-tin sphere of the target atom, Ψ_p is a regular p-solution of radial Schrödinger equation, and outside the muffin-tin sphere, Ψ_p is given by

$$\Psi_p(E, r) = [\cos\delta_p(E)]j_p[(E - V_0)^{\frac{1}{2}}r] - [\sin\delta_p(E)]n_p[(E - V_0)^{1/2}r]$$

where $\delta_p(E)$ is the p-phase shift and V_0 is the muffin-tin zero of the potential. Because $\langle\Phi_s|r|\Phi_s\rangle \ll \langle\Psi_p|r|\Psi_p\rangle$, the actual size of the muffin-tin sphere is of little importance in computing $\langle\Phi_s|r|\Psi_p\rangle$.

Therefore, the x-ray absorption cross section due to the dipole transition may be simply obtained from the p-projected DOS of the target atom (Ti) and terms dependent only on the potential, such as phase shifts.

To see the size of the quadrupole transition contribution to the pre-edge features in the Ti K-edge x-ray absorption spectrum, we have also calculated the quadrupole cross section within the multiple scattering theory [13], using the muffin-tinized self-consistent LMTO–ASA potentials. The calculations were carried out in the cluster approximation with a quadrupole adapted version of the Durham–Vvedensky program [15]. A cluster of four shells centred at the Ti site was used. The cluster used is perhaps not large enough to take the solid state effects (or band effects) fully into account. However, the significant features (if any) due to 'dipole forbidden' transitions such as $1s \rightarrow 3d$ or $1s \rightarrow 4s$, should show up in these quadrupole calculations.

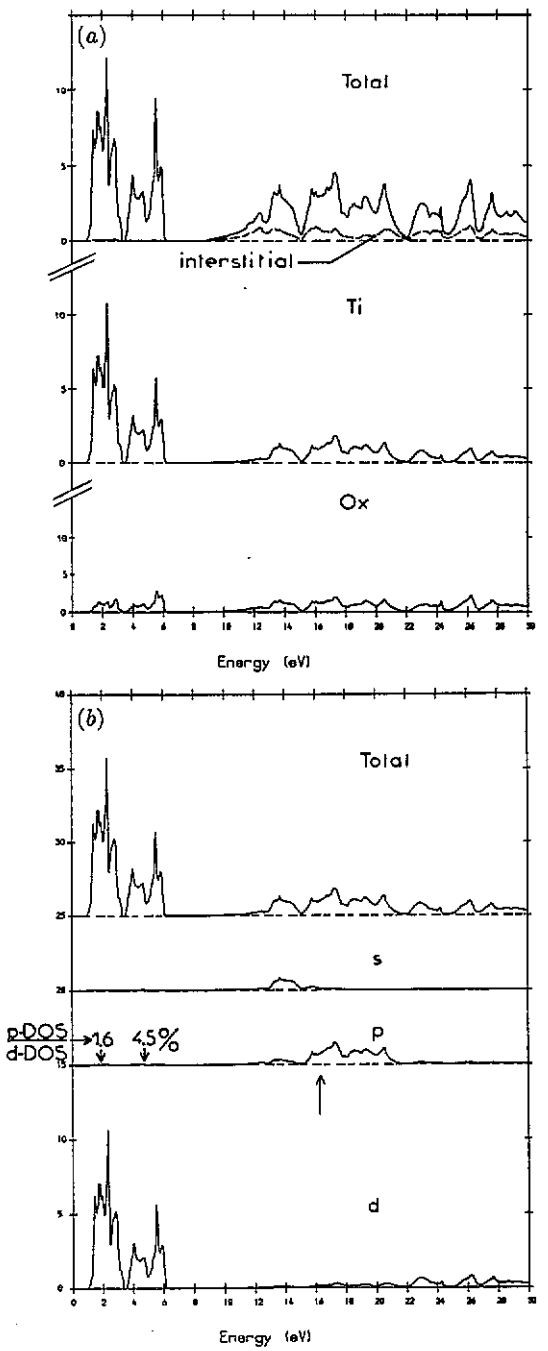

Figure 4. (*a*) Site-decomposed and (*b*) Ti *L*-decomposed DOS functions above the Fermi level. The arrow in (*b*) indicates the energy position of the maximum of the theoretical x-ray spectrum (see figure 5(*a*)).

4.2. Results and discussion

The x-ray absorption cross section calculated from the DOS (equation (3)) with an

energy convolution of 1.3 eV is shown in figure 5(*a*). Only the features before the absorption edge and the edge itself have been calculated since the results at the higher energies are less reliable (as mentioned in section 3.3). The calculated XAS cross section due to electric quadrupole transitions is not shown here because it is negligibly small (less than 0.5% of the edge intensity).

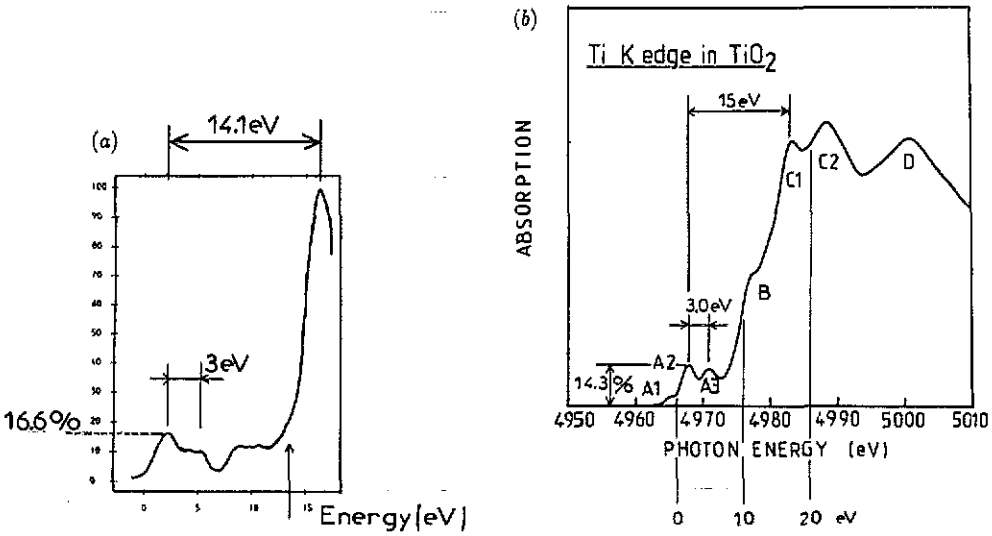

Figure 5. (*a*) The calculated x-ray absorption cross section due to the electric dipole transitions (see section 4). the arrow indicates the energy position of the maximum on the s-decomposed DOS function (see figure 4(*b*)). (*b*) Experimental spectrum together with important parameters for comparison with the calculation.

The most puzzling features in the XAS at the Ti K-edge in TiO_2 have been the first transitions just before the main edge. The intensity of these pre-edge features is remarkable, reaching about 14.3% of the full edge intensity [16]. From the atomic point of view, they can only come from the 'dipole forbidden' Ti 1s $\rightarrow$ 3d transitions. However, the intensity of these quadrupole transitions is expected to be very weak, as is confirmed by our quadrupole calculations. Therefore, the pre-edge features cannot be due to the 1s $\rightarrow$ 3d quadrupole transitions. It is thus suggested that some of these pre-edge features may result from the 'band' effects. From the band point of view, in non-cubic solids such as TiO_2, a significant component of p-symmetry (the B_{iu} symmetry in the D_{2h} point group, the Ti site symmetry group) may be due to a weak anti-symmetric combination of neighbouring Ti 3d (or 4s) orbitals and the 4p orbitals of the central Ti atom. This explains the discernible pre-edge features found in our dipole XAS (figure 5(*a*)).

We note that there are two interesting features appearing in the pre-edge region of the theoretical XAS (figure 5(*a*)). The first maximum at about 2 eV corresponds to the transitions to the first conduction bands. It is followed by a plateau centred at about 5 eV. The intensity of this feature is high, reaching 16% of the edge intensity. Since the conduction bands are of mainly Ti d character (as shown in figure 4(*b*)), these interesting features arise from the small Ti p-component (about 1.6 and 4.5%) of the conduction bands due to the Ti d–p mixing mentioned above. The intensity of this feature is enhanced by the strong energy localization of the d-dominated conduction bands (see figure 4(*b*)).

Another feature appears at about 10 eV. The intensity of this second feature is nearly the same as the previous one. This feature arises from the transitions to the bottom of the higher conduction bands where a rather large Ti s–p mixing is found. The main structure (i.e the absorption edge) peaks at 16.4 eV (as indicated in figure 4(*b*) by an arrow) and merges with the second pre-edge feature.

Comparison of the calculated and observed (shown in figure 5(*b*)) x-ray absorption spectrum reveals several interesting discrepancies. First, three peaks in the observed spectrum are clearly separated from the edge (A1–A3) whilst only two are found in the calculated spectrum. One may assign the observed peaks A2 and A3 to the electric dipole transitions to the conduction bands, as revealed in our calculated spectrum (figure 5(*a*)). Indeed, the intensities and the widths of these features in the calculated and observed spectra are in good agreement. The energy gap between the first feature and the main peak in figure 5(*a*) (14.1 eV) is also in good agreement with the separation between A2 and C1 (15 eV). However, the shapes are somehow different. The first observed peak (A1) appears to be unaccounted for within the present dipole, one-electron approximation. Secondly, the calculated absorption edge is different from the experimental one, i.e. a shoulder (B) appears clearly in the unmeasured spectrum which is absent in the former. This structure is therefore not due to the dipole transitions. It was suggested in the past that feature B may arise from quadrupole 1s $\rightarrow$ 4s transitions. However, it has been shown in this work and elsewhere [17, 18] that the magnitude of the quadrupole transitions is much too small to account for the observed shoulder B. This gives some support to the assumption that shoulder B is perhaps related to the presence of the core hole potential.

5. Conclusion

The electronic band structure of rutile TiO_2 has been calculated using the LMTO method. The results of this calculation show, among other things, that there is strong mixing between Ti and O in the valence band region. This contradicts the general assumption often made that TiO_2 is an ionic compound. The same conclusion has also been obtained for other rutile compounds by Svane and Antoncik [14]. Another interesting result is the complex nature of the band gap transitions: the direction and indirection gap transition are almost degenerate.

The Ti K-edge x-ray absorption spectrum due to the electric quadrupole transitions as well as dipole transitions has also been calculated. Since these calculations are based on band structure data, they complement Grune's interpretation [19] of the x-ray spectra with the help of the cluster calculation by Tossel *et al* [20], and may be more reliable close to threshold.

Comparison of our calculations with experiments suggests that pre-edge peaks A2 and A3 in the XAS at the Ti K-edge may be satisfactorily accounted for by the band theory. These peaks are due to electric dipolar transitions (1s $\rightarrow$ 4p) to states in which the non-cubic environment allows state density of p character to be formed from a combination of Ti d-orbitals. Nevertheless, other pre-edge features such as peak A1 and shoulder B cannot be explained within the band model with the dipole approximation. Our quadrupole calculations show that they are not due to 'dipole-forbidden' transitions such as Ti 1s $\rightarrow$ 3d, either. Further calculations taking those many-electron effects not included in the present band theory (core hole effects, multiplet effects, etc) into account may be useful in elucidating the origins of these pre-edge features.

References

[1] Poumellec B 1986 *Thesis* No 3179, Université d'Orsay
[2] Vos K and Krusemeyer H 1974 *Solid State Commun.* **15** 949
[3] Daude N, Gout C and Jouanin L 1977 *Phys. Rev.* B **15** 3229
[4] Vos K 1977 *J. Phys. C: Solid State Phys.* **10** 3917
[5] Gay J G, Albers W A and Arlinghaus F J 1968 *J. Phys. Chem. Solids* **29** 1449
[6] Blanchin M G, Vicario E and Ploc R A 1977 *J. Appl. Crystallogr.* **10** 228
[7] Andersen O K 1975 *Phys. Rev.* B **12** 3060
Skriver H L 1984 *The LMTO Method* (Berlin: Springer)
[8] von Barth U and Hedin L 1972 *J. Phys. C: Solid State Phys.* **55** 1629
[9] Jepsen O and Andersen O K 1971 *Solid State Commun.* **9** 1763
Lehman G and Taut M 1971 *Phys. Status Solidi* b **54** 469
[10] Pascual J, Camassel J and Mathieu H 1977 *Phys. Rev. Lett.* **39** 1490
[11] Mathieu H, Pascual J and Camassel J 1978 *Phys. Rev.* B **18** 6920
[12] Muller J E and Wilkins J W 1984 *Phys. Rev.* B **29** 4331
[13] Durham P J 1984 *The Electronic Structure of Complex Systems* ed P Phariseau and W M Temmerman (New York: Plenum)
[14] Svane A and Antoncik E 1977 *J. Phys. Chem. Solids* **48** 171
[15] Durham P J and Pendry J B 1982 *Comput. Phys. Commun.* **25** 193
Vvedensky D D and Pendry J B 1986 *Comput. Phys. Commun.* **40** 421
[16] Poumellec B, Cortes R, Tourillon G and Berthon J 1991 *Phys. Status Solidi* b **164** 319
[17] Hildebrandt G, Stephensen J D and Wagenfeld H 1975 *Z. Naturf.* a **30** 698
[18] Kosugi N, Yokoyama T, Asakura K and Kuroda H 1984 *Chem. Phys.* **91** 249
[19] Grunes L A 1983 *Phys. Rev.* B **27** 2111
[20] Tossel J A, Vaughan D J and Johnson K H 1974 *Am. Mineral.* **59** 319